JOURNAL OF GEOPHYSICAL RESEARCH, VOL. 122, XXXX, DOI:10.1029/,

Toward an integrated view of ionospheric plasma instabilities: 3. Explicit growth rate and oscillation frequency for arbitrary altitude

Roman A. Makarevich[1]

R. A. Makarevich, Geophysical Institute, University of Alaska Fairbanks, 903 Koyukuk Drive, PO Box 757320, Fairbanks, AK, 99775-7320, USA. (rmakarevich@alaska.edu)

[1]Geophysical Institute and Department of Physics, University of Alaska Fairbanks, Fairbanks, AK, USA.

Abstract. General analytic expressions are derived for the growth rate γ and oscillation frequency in the ion frame ω_r' of unstable plasma waves generated by ionospheric plasma instabilities including the Farley-Buneman instability (FBI) and the gradient-drift instability (GDI). The explicit expressions are developed for arbitrary altitude and scales in the local approximation. Limits of applicability are carefully considered focusing on the dependence on the electron density gradients $\mathbf{G} = \nabla n/n$ and wavelengths λ. It is shown that the key parameter that controls the applicability is the growth rate γ normalized to the ion collision frequency ν_i, with the developed expressions being valid for slow growths $\gamma/\nu_i < 0.1$. It is also shown that the commonly used assumption about the equivalency of the wave phase velocity $V_{\rm ph}$ and the plasma drift velocity V_d fails in the F region at gradients as weak as $G = 10^{-5}$ m^{-1}. The developed analytic expressions for arbitrary altitude/scale offer a straightforward way of reconciling various altitude- and scale-specific cases (e.g. FBI/GDI modes in the E region), with the often-neglected ion inertia shown to play a critical role in the reconciliation. The new ion inertia effect is found to be represented by the quantity $(\nu_i^2 + \omega_r'^2)^{-1}$ in the growth rate expression. The effect is found to reduce the standard FBI factor and amplify the GDI factor and, due to the inverse relationship with the ion inertia, the effect becomes progressively stronger at larger altitudes and/or wavelengths.

1. Introduction

Greater physical insight is often obtained when seemingly different processes are considered within the same formalism. Formation of plasma waves or irregularities in the Earth's ionosphere is no exception, with successful theoretical efforts including integration with respect to different plasma instabilities such as the Farley-Buneman instability (FBI) and the gradient-drift instability (GDI) in the ionospheric E region [*Rogister and D'Angelo*, 1970; *Sudan et al.*, 1973; *Fejer et al.*, 1975] as well as integration with respect to different altitudes [*Fejer et al.*, 1984; *Dimant and Oppenheim*, 2011b; *Makarevich*, 2014, 2016a, b].

Integrated or unified formalism of ionospheric plasma instabilities allows to derive a general dispersion relation which can be solved for the instability growth rate and wave oscillation frequency. Analytic expressions are particularly useful since they allow to analyze different destabilizing and stabilizing factors, thereby providing greater physical insight [e.g. *Dimant and Oppenheim*, 2011b]. Such expressions remain, however, difficult to develop for most general cases. Thus *Dimant and Oppenheim* [2011b] considered both FBI and GDI at an arbitrary altitude, but limited their consideration to long wavelengths. *Makarevich* [2016a, b] considered more arbitrary scales, but failed to obtain analytic expressions since dispersion relation was cubic in complex wave frequency.

In the current study, approximate explicit expressions for the growth rate and oscillation frequency are developed based on the theory by *Makarevich* [2016a, b] that provide greater insight into various destabilizing and stabilizing factors at various altitudes. The approximations employed and applicability limits are carefully considered and the developed expressions are reconciled with various limiting cases.

The paper is organized as follows. In Section 2, different forms of a general dispersion relation are presented. In Section 3, the adopted vector geometry is introduced and expressions for zeroth-order oscillation frequency are derived. In Section 4, explicit approximate expressions for the growth rate are derived from the general dispersion relation, while in Section 5 these expressions are demonstrated to be consistent with the previously considered limiting cases. Section 6 considers limits of applicability of the explicit expressions for the growth rate in terms of density gradients and wavelengths. In Section 7, explicit expressions for the oscillation frequency are derived, while their limits of applicability are considered in Section 8. Finally, in Section 9, the underlying physics of inertial effects in the instability growth rate is discussed, focusing on altitude and wavelength dependence.

2. Forms of General Dispersion Relation

In this section, four forms of a general dispersion relation that was previously derived by *Makarevich* [2016a, b] are introduced. A version of general dispersion relation that describes fundamental ionospheric plasma instabilities including FBI and GDI for arbitrary altitude in the ion frame and for nearly field-aligned irregularities (NFAI) has been derived by *Makarevich* [2016b, equation 3] as

$$(iD_i + aD_i - b)\left(\omega' - \mathbf{V}_d \cdot \mathbf{k}\right) - \hat{P}\left[\left(1 + D_i^2\right)\omega' + Ck_\perp^2\left(iD_i + aD_i - b\right)\right] = 0. \qquad (1)$$

This equation hereinafter is referred to as the **standard form** of the dispersion equation. Here $\mathbf{V}_d = \mathbf{V}_{e0} - \mathbf{V}_{i0}$ is the plasma drift velocity or the difference between the background drift velocities of electrons and ions, $\omega' = \omega - \mathbf{k} \cdot \mathbf{V}_{i0}$ is the complex wave frequency in the ion frame, $r_\alpha = \nu_\alpha / \Omega_\alpha$ is the ratio between the collision frequency ν_α and gyrofrequency $\Omega_\alpha = q_\alpha B / m_\alpha$ of a plasma species $\alpha = (i, e)$, and other quantities are defined through

$$D_i = -i\Omega_i^{-1}\omega' + r_i, \quad C = \frac{T_i + T_e}{|e|B} = \frac{C_s^2}{\Omega_i}, \quad a = \mathbf{G}\cdot\mathbf{k}_\perp/k_\perp^2,$$
$$b = -\mathbf{G}\cdot\mathbf{k}\times\hat{\mathbf{b}}/k_\perp^2, \quad \hat{\mathbf{b}} = \mathbf{B}/B, \quad \mathbf{G} = \nabla n/n. \tag{2}$$

The quantity D_i defined by *Makarevich* [2016a] is a Fourier representation of the convective derivative plus collisional term $\partial/\partial t + \mathbf{V}_{i0}\cdot\nabla + \nu_i$, normalized to the ion gyrofrequency Ω_i, C is a thermal diffusion term related to the ion-acoustic speed C_s, a and b are gradient-related quantities that are defined in that way to be small in the local approximation since they are both proportional to G/k, and $\mathbf{G}$ is a gradient strength vector. The quantity $\hat{P}$ in Eq. (1) has been defined by *Makarevich* [2016b] through

$$\hat{P} \equiv -i\hat{\psi}r_i^{-1} + ar_e - b. \tag{3}$$

under an implicit assumption of no parallel density gradients $G_\parallel = 0$. Here $\hat{\psi}$ is the anisotropy factor that depends on the ratios r_i, r_e and the aspect angle α' through

$$\hat{\psi} \equiv \psi\left(1 + r_e^{-2}y^2\right), \quad \psi \equiv -r_i r_e, \quad y \equiv k_\parallel/k_\perp \equiv \tan\alpha'. \tag{4}$$

In order to maintain exact numerical equivalence between Eq. (1) and the following equivalent forms of the dispersion relation, the assumption $G_\parallel = 0$ is lifted in the present study, with the following generalization of the quantity $\hat{P}$

$$\hat{P} \equiv -i\hat{\psi}r_i^{-1} - a\psi' r_i^{-1} - b, \quad \psi' \equiv \psi\left(1 + r_e^{-2}y^2 c/a\right), \quad c \equiv \mathbf{G}\cdot\mathbf{k}_\parallel/k_\parallel/k_\perp. \tag{5}$$

Following *Makarevich* [2016b], Eq. (1) is rewritten purely in terms of frequency-dependent quantity D_i by substituting $D_i = -i\Omega_i^{-1}\omega' + r_i$ from Eq. (2), multiplying by $i - a$ and simplifying

$$\hat{A}D_i^3 + \hat{B}D_i^2 + \hat{C}D_i + \hat{D} = 0, \qquad \textbf{[cubic form]} \tag{6}$$

with

$$\hat{A} \equiv (i-a)\,\hat{P}, \quad \hat{B} \equiv 1 + a^2 - r_i\hat{A}, \quad \hat{C} \equiv \left(i\hat{W} - r_i\right)\left(1+a^2\right) - \left(i\hat{\psi} + a\psi'\right) r_i^{-1}(i-a),$$
$$\hat{D} \equiv \left(ib\hat{W} + i\hat{\psi} + a\psi'\right)(i-a), \quad \hat{W} \equiv \Omega_i^{-1}\left(\mathbf{V}_d \cdot \mathbf{k} + \hat{P}Ck_\perp^2\right). \tag{7}$$

Equation (6) hereinafter is referred to as the cubic form of the dispersion equation. Even though $a\psi' r_i^{-1} \ll b$ and can therefore often be neglected in $\hat{P} = -i\hat{\psi}r_i^{-1} - a\psi' r_i^{-1} - b$, when working with the standard form (1) [e.g. *Makarevich*, 2016a, equation (21)], it is useful to maintain numerical equivalency between the two forms (1) and (6), which allows for easy numerical tests of the explicit expressions to be derived in the following sections.

One should also note that in deriving a similar cubic equation *Makarevich* [2016b] employed two additional restrictions: the local approximation $a^2 \ll 1$ and no parallel gradients $c = 0$. For that case, they approximated $\hat{A} \approx ab - ib + \hat{\psi}r_i^{-1}$, while $\hat{W}$ had a slightly less general quantity $\hat{P} = -i\hat{\psi}r_i^{-1} + ar_e - b$. Employing $c = 0$ in Eq. (6) is equivalent to substituting $\psi' \to \psi$, while employing $a^2 \ll 1$ results in

$$\hat{A}D_i^3 + D_i^2\left(1 - r_i\hat{A}\right) + D_i\left[i\hat{W} - r_i + \hat{\psi}r_i^{-1} + ia\left(\hat{\psi} - \psi\right) r_i^{-1}\right] - (1+ia)\,b\hat{W} - \hat{\psi} + ia\left(\psi - \hat{\psi}\right) = 0. \tag{8}$$

This differs from Eq. (9) of *Makarevich* [2016b] by small factors proportional to $\psi - \hat{\psi}$ which reduce to zero for purely perpendicular propagation $k_\parallel = 0$. In the following analysis, a more general and accurate cubic equation (6) will be used to obtain exact numerical solutions in D_i and therefore in ω' from Eq. (2). These solutions will be, in turn, used to test explicit expressions for ω' that are developed in the following sections.

For further analysis it is also convenient to divide the standard form (1) by iD_i+aD_i-b and rewrite using a new frequency-dependent quantity Z as

$$\omega' = \mathbf{V}_d \cdot \mathbf{k} - \left(Z\omega' + iCk_\perp^2\right)\left(\hat{\psi}r_i^{-1} - ib - ia\psi' r_i^{-1}\right) \quad \textbf{[iterative form]}, \tag{9}$$

$$Z \equiv \frac{1+D_i^2}{D_i - iaD_i + ib}. \tag{10}$$

This form hereinafter is referred to as the iterative form of the dispersion equation, since it has the form $\omega' = f(\omega')$ and can be solved iteratively as $\omega'_{n+1} = f(\omega'_n)$, similar to *Makarevich* [2016a].

The fourth and final form of the dispersion relation is obtained by taking $\Re$ and $\Im$ of Eq. (9) and writing out explicitly all terms in the growth rate $\gamma = \Im\omega'$. The detailed derivation is given in Appendix A, with resulting equations for the oscillation frequency ω'_r and the growth rate γ being quadric in γ

$$\omega'_r D_0 = \left(X_0 + X_1\gamma + X_2\gamma^2\right)\omega'_{r0} - \gamma\Omega_1 - \gamma^2\Omega_2 - \gamma^3\Omega_3 - \gamma^4\Omega_4. \tag{11}$$

$$\gamma^4\Gamma_4 + \gamma^3\Gamma_3 + \gamma^2\Gamma_2 + \gamma\Gamma_1 = \Gamma_0 \quad \textbf{[quadric form]}. \tag{12}$$

Here quantities $D_0, X_j, \Omega_j, \Gamma_j$ depend on the oscillation frequency ω'_r, as given in Appendix A. Together, Eqs. (11–12) are referred to as the **quadric form** (in γ) of the dispersion relation.

One should note that all four forms (1), (6), (9), and (11–12) are equivalent. While finding solutions is numerically preferable from the cubic form (6) [*Makarevich*, 2016b], in the following sections the quadric form (11–12) is approximated to obtain explicit expressions for ω_r' and γ.

3. Vector Geometry and Zeroth-Order Oscillation Frequency ω_{r0}'

In this section, vector geometry and angle definitions are introduced and several parameters of interest are evaluated for arbitrary altitude, with a particular focus on the differential drift speed V_d and zeroth-order oscillation frequency that has been defined in Appendix A as

$$\omega_{r0}' \equiv \mathbf{V}_d \cdot \mathbf{k} - \left(b + a\psi' r_i^{-1}\right) C k_\perp^2. \tag{13}$$

In the present study, the same vector geometry and model ionospheric parameters (i.e. $\nu_i, \Omega_i, \nu_e, \Omega_e, C_s$) are adopted as in *Makarevich* [2016b, 2017]. Figure 1 illustrates the adopted geometry. This geometry is completely general since the choice of the coordinate system with the x axis along the background electric field $\mathbf{E}$ preserves generality. The angle definitions are also the same as in *Makarevich* [2017], with an additional angle β defined as

$$\beta \equiv \tan^{-1} r_i. \tag{14}$$

The exact vector directions in Figure 1 refer to an E-region altitude of 110 km where $r_i \approx 5$. For the F region, $r_i \ll 1$ and $\beta \approx 0$. The flow angle θ is defined as the angle between the wavevector $\mathbf{k}$ and $\mathbf{V}_d$ or, in terms of the new "phase" angle β, Figure 1, as

$$\theta = \pi - \alpha - \beta. \tag{15}$$

From Appendix B, the zeroth-order oscillation frequency can be written as

$$\omega'_{r0} \approx s_i r_i \left(r_i \mathbf{V}_E - \frac{\mathbf{E}_{0\perp}}{B} \right) \cdot \mathbf{k} + r_e^{-1} k_\parallel \frac{E_{0\parallel}}{B}, \qquad s_i = \left(1 + r_i^2\right)^{-1}. \tag{16}$$

This equation can be simplified by substituting $r_i = \tan\beta$ from Eq. (14) into the second r_i factor and employing the coordinate system of Figure 1 with $\mathbf{E}_{0\perp}/B = V_E \hat{\mathbf{e}}_x$, $\mathbf{V}_E = V_E \hat{\mathbf{e}}_y$, and $\mathbf{k} = k_\perp (\cos\alpha \hat{\mathbf{e}}_x + \sin\alpha \hat{\mathbf{e}}_y) - k_\parallel \hat{\mathbf{e}}_z$ to become

$$\omega'_{r0} \approx -s_i^{1/2} r_i V_E k_\perp \cos(\alpha + \beta) + r_e^{-1} k_\parallel \frac{E_{0\parallel}}{B}. \tag{17}$$

From the above form, it is easy to see that β represents a phase factor as it is added to α in the argument of the cosine function. Eq. (17) is also useful in demonstrating the importance of two special cases: $\theta = 0$ and $\alpha = 0$. In the first case, the differential plasma flow $\mathbf{V}_d$ is parallel to the direction of propagation $\mathbf{k}$, Figure 1. In this case ω'_{r0} reaches its maximum value since $\cos(\alpha + \beta) = \cos\pi = -1$ and

$$\omega'_{r0,\max} \approx s_i^{1/2} r_i V_E k. \tag{18}$$

In the case of $\alpha = 0$, it is the electric field that is parallel to the propagation direction, Figure 1, and in this case expression for ω'_{r0} also simplifies since $\cos\beta = \cos\tan^{-1} r_i = \left(1 + r_i^2\right)^{-1/2} = s_i^{1/2}$. A similar simplification also occurs for $\alpha = \pi$ so that

$$\omega'_{r0}(\alpha = 0, \pi) \approx \mp s_i r_i V_E k. \tag{19}$$

A similar analysis can be carried out in terms of the differential drift speed $V_d \sim s_i^{1/2} r_i V_E$ from Eq. (B6) and the flow angle θ from Eq. (15) as

$$\omega'_{r0} \sim V_d k \cos\theta. \tag{20}$$

The end result of $\omega'_{r0} \sim \mathbf{V_d} \cdot \mathbf{k}$ is a well-familiar expression, but it is important to understand that this is an approximation. In particular, it does not contain any gradient terms; these can be neglected for most gradient conditions, as discussed in Appendix B. In the following analytic derivations, Eqs. (18) and (19) will be used in the order-of-magnitude (OOM) analysis. In this analysis, magnitudes of different terms are compared and approximate expressions (18)–(20) are substituted into terms containing ω'_{r0} to determine which terms can be neglected, e.g. Appendix C. For all numerical calculations, however, the original exact definition for ω'_{r0} (13) will be used.

4. Explicit Expression for the Growth Rate

In this section, an explicit approximate expression is developed for the growth rate γ. We start from the quadric equation (12) and employ the following approximations:

$$G \ll k, \qquad \textbf{[local approximation]} \tag{21}$$

$$|\gamma| \ll \nu_i. \qquad \textbf{[slow growth approximation]} \tag{22}$$

The physical meaning of these approximations is as follows. In the local approximation, the gradient strength is much smaller than the wavenumber or, alternatively, the gradient scale length is much larger than the wavelength, and the dispersion relation is valid at any point in the plasma, using the local values of the plasma parameters. In the slow growth approximation, the instability growth rate is much smaller than collision frequency, and only lower-order terms in γ from convective derivative and related quantity D_i contribute to the dispersion relation and equation on γ.

The local approximation allows to neglect all terms quadratic in G^2, i.e. a^2, b^2, ab, in expressions for Γ_j (A18). In notations of Appendix A, $\Gamma_j = \Gamma_{j,0} + \Gamma_{j,1} + \Gamma_{j,2} \approx \Gamma_{j,0} + \Gamma_{j,1}$, where the first term $\Gamma_{j,0}$ is gradient-free, while the second term $\Gamma_{j,1}$ has parts proportional to b and a. The slow growth approximation allows to neglect two higher-order terms in γ in Eq. (12) which becomes quadratic

$$\bar{\gamma}^2 \Gamma_2 + \bar{\gamma} \Gamma_1 = \Gamma_0, \tag{23}$$

with the bar notation introduced to specify that this is an exact solution of the quadratic equation which approximates a solution of the quadric equation γ. From Eq. (A18), the coefficients Γ_j are given by

$$\begin{aligned}
\Gamma_0 &= \hat{\psi} r_i^{-1} \left[\omega_r'^2 \Omega_i^{-1} (I-1) - C k_\perp^2 I\right] + b \omega_r' r_i \left[1 + 2\hat{\psi} + I + \hat{\psi} r_i^{-2} \left(1 - I + 2C k_\perp^2 \Omega_i^{-1}\right)\right] + a \omega_r' \left(\psi' - \hat{\psi}\right) (1 + I \\
\Gamma_1 &= I + \hat{\psi} \left(1 + I - 2\omega_r'^2 \Omega_i^{-2} + 2C k_\perp^2 \Omega_i^{-1}\right) - 2b \omega_r' \Omega_i^{-1} \left(1 + 2\hat{\psi} + r_i^2 + I\right) + 2a \left(\hat{\psi} - \psi'\right) r_i^{-1} \omega_r' \Omega_i^{-1} \left(I + r_i^2\right), \\
\Gamma_2 &= r_i \Omega_i^{-1} \left[2 + 3\hat{\psi} + \hat{\psi} r_i^{-2} \left(1 + C k_\perp^2 \Omega_i^{-1}\right)\right] + \omega_r' \Omega_i^{-2} \left[5a \left(\hat{\psi} - \psi'\right) - b r_i \left(5 + 3\hat{\psi} r_i^{-2}\right)\right],
\end{aligned} \tag{24}$$

with

$$I \equiv r_i^2 + \omega_r'^2 \Omega_i^{-2} = \left(\nu_i^2 + \omega_r'^2\right) \Omega_i^{-2}. \tag{25}$$

A solution of Eq. (23) is given by

$$\bar{\gamma} = \frac{2\Gamma_0 \Gamma_1^{-1}}{1 + \sqrt{1 - 4\rho}}, \tag{26}$$

where we used an alternative expression for the quadratic equation root [*Press et al.*, 1992, equation (5.6.5)] and introduced a new definition

$$\rho \equiv -\Gamma_2 \Gamma_0 \Gamma_1^{-2}. \tag{27}$$

In principle, one can also consider a linear solution $\Gamma_0 \Gamma_1^{-1}$ (essentially a case of $\rho = 0$), but an important (quadratic) correction can also be obtained analytically by expanding the square root for $|\rho| < 1$

$$\bar{\gamma} \approx \frac{2\Gamma_0 \Gamma_1^{-1}}{1 + 1 - 2\rho} = \frac{\Gamma_0}{\Gamma_1 - \rho \Gamma_1}. \tag{28}$$

Here the second term in the denominator represents a quadratic correction to the linear solution Γ_0/Γ_1. Further simplification can be obtained by factoring out the typically dominant term I from the denominator $\Gamma_1 - \rho\Gamma_1 \equiv I\left[1 + \epsilon - \rho\left(1 + \epsilon\right)\right]$ and treating both ρ and ϵ as small corrections, with the resulting approximate expression being

$$\widetilde{\gamma} = \frac{\hat{\psi} r_i^{-1}\left[\omega_r'^2 \Omega_i^{-1}\left(1 - I^{-1}\right) - C k_\perp^2\right] + b\omega_r' r_i \left(1 + I^{-1} + 2\hat{\psi} r_i^{-2} I^{-1} C k_\perp^2 \Omega_i^{-1}\right) + a\omega_r' \left(\psi' - \hat{\psi}\right)\left(1 + I^{-1}\right)}{1 + \hat{\psi}\left(1 + I^{-1}\right)}, \tag{29}$$

where a notation $\widetilde{\gamma}$ is introduced to distinguish this approximate solution from their quadric γ or quadratic $\bar{\gamma}$ counterparts. This expression can be further simplified by neglecting the last two terms in the numerator. The OOM analysis of these terms carried out in Appendix C shows that losses in applicability associated with these terms are relatively small.

If both of the last two terms in Eq. (29) can be neglected, the growth rate takes a relatively simple form

$$\widetilde{\gamma} = \frac{\hat{\psi} r_i^{-1} \Omega_i^{-1} \left[\omega_r'^2 \left(1 - I^{-1}\right) - C_s^2 k_\perp^2 \right] + b \omega_r' r_i \left(1 + I^{-1}\right)}{1 + \hat{\psi} \left(1 + I^{-1}\right)}, \tag{30}$$

where we used the identity $C = C_s^2 \Omega_i^{-1}$ from Eq. (2).

The final approximate form of the growth rate is obtained by substituting ω_r' from Eq. (17) and rewriting the gradient term b in terms of angles α and χ defined in Section 3 as

$$b = -\mathbf{G} \cdot \mathbf{k} \times \hat{\mathbf{b}} / k_\perp^2 = G k_\perp^{-1} \sin\left(\alpha - \chi\right). \tag{31}$$

For the case of the purely field-aligned irregularities (PFAI), the growth rate becomes

$$\widetilde{\gamma} \approx \frac{\hat{\psi} \nu_i^{-1} k_\perp^2 \left[s_i r_i^2 V_E^2 \cos^2\left(\alpha + \beta\right) \left(1 - I^{-1}\right) - C_s^2 \right] + G V_E f s_i r_i^2 \left(1 + I^{-1}\right)}{1 + \hat{\psi} \left(1 + I^{-1}\right)}, \tag{32}$$

where a new function f has been defined as

$$f\left(\alpha, \beta, \chi\right) \equiv -s_i^{-1/2} \cos\left(\alpha + \beta\right) \sin\left(\alpha - \chi\right). \tag{33}$$

The function f describes a directional dependence of the gradient term. Since $\cos\beta = s_i^{1/2}$, it simplifies for a representative configuration with $\chi = \pi/2$, $\alpha = 0, \pi$ as $f\left(0, \beta, \pi/2\right) = f\left(\pi, \beta, \pi/2\right) = 1$. Similarly, $f = 1$ when $\cos\left(\alpha + \beta\right) = -1$ or, in terms of the flow angle defined through Eq. (15), when $\theta = 0$.

5. Limiting Cases for the Growth Rate Expression

5.1. Limiting Case 1: *E* region

In the E region, $r_i^2 \gg 1$ and therefore $I^{-1} \ll 1$ from its definition (25). In this case, Eq. (30) becomes

$$\gamma^E = \frac{\hat{\psi} r_i^{-1} \Omega_i^{-1} \left(\omega_r'^2 - C_s^2 k_\perp^2\right) + b\omega_r' r_i}{1+\hat{\psi}}, \tag{34}$$

which is is exact agreement with the standard FBI/GDI expression in the E region, e.g. Eq. (22) of *Makarevich* [2016a].

5.2. Limiting Case 2: Long Wavelengths for Arbitrary Altitude

In this case, $\omega_r' \ll \nu_i$ or $\omega_r' \Omega_i^{-1} \ll r_i$. Hence from definition of I (25), $I^{-1} \approx r_i^{-2}$ and

$$\gamma_{\rm LW} = \frac{\hat{\psi} r_i^{-1} \left[\omega_r'^2 \Omega_i^{-1} \left(1 - r_i^{-2}\right) - C k_\perp^2\right] + b\omega_r' r_i \left(1 + r_i^{-2}\right)}{1 + \hat{\psi}\left(1 + r_i^{-2}\right)}, \tag{35}$$

where a subscript LW indicates long wavelengths. This is an arbitrary-altitude expression applicable in the long-wavelength limit. It is demonstrated below that it is consistent with the growth rate expression derived by *Dimant and Oppenheim* [2011b]. We first make the following identifications between their and our notations

$$\begin{aligned}
&\kappa_\alpha = r_\alpha^{-1},\\
&\psi_{\vec{k}} = \psi\left[1 + \left(1 + r_i^{-2}\right)\left(1 + r_e^{-2}\right) y^2\right] \approx \psi\left[1 + \left(1 + r_i^{-2}\right) r_e^{-2} y^2\right] = \hat{\psi}\left(1 + r_i^{-2}\right) - \psi r_i^{-2},\\
&\Omega_{\vec{k}1}^{(i)} = \frac{\mathbf{k}\cdot\mathbf{V_d}}{1+\psi_{\vec{k}}} \approx \frac{\omega_{r0}'}{1+\psi_{\vec{k}}} \equiv \omega_{r\vec{k}}'.
\end{aligned} \tag{36}$$

Here the approximation $|r_e| \gg 1$ was used and a shorthand $\omega_{r\vec{k}}'$ was introduced for the frequency. It will be demonstrated in Section 7 that $\omega_{r\vec{k}}'$ is a better approximation to ω_r' than ω_{r0}' which we have previously used in our OOM analysis.

Eqs. (A30)–(A32) of *Dimant and Oppenheim* [2011b] are next rewritten in our present notations and a case of fully-magnetized electrons is considered $|r_e| \ll 1$. In this case, Eqs.

(A30)–(A32) of *Dimant and Oppenheim* [2011b], when combined into a single growth rate expression, become

$$\gamma_{\mathrm{D\&O}} = \frac{\hat{\psi} r_i^{-1} \left[\omega_{r\vec{k}}'^2 \Omega_i^{-1} \left(1 - r_i^{-2}\right) - C k_\perp^2\right] + \omega_{r\vec{k}}' r_i \left(1 + r_i^{-2}\right) \left[b - r_e^{-1} y c + r_e^{-1} a y^2\right]}{1 + \hat{\psi}\left(1 + r_i^{-2}\right) - \psi r_i^{-2}}, \quad (37)$$

where a subscript D&O is introduced to indicate that these results are by *Dimant and Oppenheim* [2011b]. One should note that Eq. (37) contains one extra term of $r_e^{-1} a y^2$ which is missing from their Eqs. (A34)–(A35) which are also written for the fully-magnetized electrons case. This term, together with another term $-r_e^{-1} y c$, are not present in our expression (35). Both are present, however, if a more general Eq. (29) is written in the long-wavelength limit. Thus the growth rate from *Dimant and Oppenheim* [2011b] represented by Eq. (37) is fully consistent with the long-wavelength limit of expression (29) except for an additional term $-\psi r_i^{-2}$ in the denominator.

It has been previously noted that for arbitrary ion magnetization ratio r_i (i.e. arbitrary-altitude case), the generalized anisotropy parameter $\psi_{\vec{k}}$ replaces the product $\hat{\psi}\left(1 + r_i^{-2}\right)$ but the difference is of the order of ψr_i^{-2} and therefore small [*Dimant and Oppenheim*, 2011a, Eqs. (34a,b) and Section 3.1]. However, the factor $\hat{\psi}\left(1 + r_i^{-2}\right)$ is already appropriate for any r_i and it can be approximated as $\psi_{\vec{k}}$ only for $r_i^{-2} \ll 1$. This is also the factor that appears in the growth rate from *Dimant and Milikh* [2003] (their equation 5) which was written for the gradient-free case and is equivalent to

$$\gamma_{\mathbf{k}} = \frac{\hat{\psi} r_i^{-1} \left[\omega_{r\vec{k}}'^2 \Omega_i^{-1} \left(1 - r_i^{-2}\right) - C k_\perp^2\right]}{1 + \hat{\psi}\left(1 + r_i^{-2}\right)}. \quad (38)$$

This expression is fully consistent with our Eq. (35) since $b = 0$ for the gradient-free case.

5.3. Limiting Case 3: Long Wavelengths in the F region

A particular case of interest in the long-wavelength limit is in the F region where $r_i^{-2} \gg 1$ and where Eq. (35) becomes

$$\gamma_{\mathrm{LW}}^F = \frac{b\omega_r' r_i^{-1}}{1+\hat{\psi} r_i^{-2}} - \frac{\hat{\psi} r_i^{-1} k_\perp^2 \left(C + \omega_r'^2 k_\perp^{-2} \Omega_i^{-1} r_i^{-2}\right)}{1+\hat{\psi} r_i^{-2}}. \tag{39}$$

One can rewrite Eq. (39) by using identities $\hat{\psi} r_i^{-1} = -r_e + \psi^{-1} r_i y^2$, $1+\hat{\psi} r_i^{-2} = \psi^{-1}\left(\psi + y^2\right)$ and $\omega_r' \approx \omega_{r0}'^F$ from Eq. (B9) as

$$\gamma_{\mathrm{LW}}^F = -\frac{b}{\psi + y^2}\left(\psi \frac{\mathbf{E}_{0\perp}}{B}\cdot\mathbf{k} + \frac{E_{0\parallel} k_\parallel}{B}\right) + \left(r_e k_\perp^2 - \frac{r_i k_\parallel^2}{\psi + y^2}\right)\left(C + \omega_r'^2 k_\perp^{-2} \Omega_i^{-1} r_i^{-2}\right). \tag{40}$$

This agrees with Eq. (27) of *Makarevich* [2016a] except for the term $\omega_r'^2 k_\perp^{-2} \Omega_i^{-1} r_i^{-2}$ that is added to C.

The first term in Eq. (39) is gradient-dependent but wavelength-independent to zeroth order, since $b \propto G/k$ and $\omega_r' \propto k$ to zeroth order, Section 3. The second term in Eq. (39), on the other hand, decreases with the wavelength as $\lambda^{-2} = k^2$. If it is neglected as well as the typically small term $\hat{\psi} r_i^{-2}$ in the denominator, Eq. (39) takes a simple form

$$\gamma_{\mathrm{LW}}^F \approx b\omega_r' r_i^{-1}. \tag{41}$$

Evaluating ω_r' from Eq. (16) and using $s_i \approx 1$ as is appropriate in the F region, one obtains

$$\gamma_{\mathrm{LW}}^F \approx b\left(r_i \mathbf{V}_E - \frac{\mathbf{E}_{0\perp}}{B}\right)\cdot\mathbf{k}, \tag{42}$$

which is in agreement with Eq. (28) from *Makarevich* [2016a]

$$\gamma = \frac{b}{1+\psi}\left(R\mathbf{V}_E - \frac{\mathbf{E}_{0\perp}}{B}\right)\cdot\mathbf{k} \tag{43}$$

considering that $R = (r_i + r_e)/(1+\psi) \approx r_i$ and $\psi \ll 1$ in the F region.

6. Limits of Applicability: Growth Rate

In this section, limits of applicability of the developed expressions for the growth rate are considered. Figure 2 shows a dependence on the wavelength λ and gradient strength G of (a) the exact quadric values γ, Eq. (12), (b) the quadratic values $\bar{\gamma}$, Eq. (26) and (c) the approximate values $\widetilde{\gamma}$, Eq. (29) at an altitude of 300 km, representative combination of gradient and propagation directions $\chi = \pi/2$, $\alpha = 0$, and the PFAI case $\alpha' = 0$. In Figure 2a, the normalized growth rate itself is shown γ/ν_i, while in Figures 2b and 2c, the differences with respect to the exact values γ are shown, i.e. $(\bar{\gamma} - \gamma)/\nu_i$ and $(\widetilde{\gamma} - \gamma)/\nu_i$, respectively. Figures 2d–2f show the same, but for an E-region altitude of 110 km. The exact values γ were obtained by numerically solving the cubic form of the dispersion relation (6) as described by *Makarevich* [2016b], while the $\bar{\gamma}$ and $\widetilde{\gamma}$ values were obtained by numerically solving exact quadratic Eq. (26) and finding its approximate solution from Eq. (29), respectively. In these calculations of the quadratic $\bar{\gamma}$ and approximate $\widetilde{\gamma}$ values, we used the exact frequencies ω_r' which were also obtained from numerical solutions of Eq. (6).

Also shown in Figure 2 are contours of $\gamma = 0$ (grey-white dashed line), $\gamma/\nu_i = 0.5$ (pink dashed), and $\bar{\gamma} = \gamma$ or $\widetilde{\gamma} = \gamma$ (white dotted) from the above described numerical analysis. In addition, the pink solid lines show critical gradients $G_\kappa(\lambda), \kappa = \pm 0.001, 0.01, 0.1$ from analytic expressions (D4) derived in Appendix D, and the red solid lines show $G = \kappa k$. In the corners defined by the last set of lines the local approximation $G \ll k$ or $G\lambda \ll 1$, Eq.

(21), becomes progressively less applicable since $G/k = 0.001$ on the leftmost red line, $G/k = 0.01$ on the middle red line, and $G/k = 0.1$ on the rightmost red line. Similarly, the slow growth approximation $|\gamma| \ll \nu_i$, Eq. (22), becomes less applicable further away from the $\gamma = 0$ line.

From Figures 2a and 2d, the analytic expressions for gradients G_κ work well to describe the growth rate magnitudes for the slow growth case, i.e. they follow the contours of constant γ/ν_i. This is fully expected since they were derived under this approximation. From Figure 2a, the growth in the F region is slow $|\gamma|/\nu_i \leq 0.1$ (between outmost pink lines) except at short scales ($\lambda \leq 2$ m) or strong gradients $G \geq 2 \times 10^{-5}$. In the E region, the growth is slow for most gradients and wavelengths of interest.

From Figure 2b and 2e, solutions of the quadratic equation $\bar{\gamma}$ agree well with exact values γ except at large positive growth rates (blue color). As a rough guide, Figure 2b shows the value of $\gamma/\nu_i = 0.5$ by the dashed pink line and large disagreements start above it. In the E-region, there are no significant disagreements in the domain of interest, since lines of $\gamma/\nu_i = 0.5$ and even $\gamma/\nu_i = 0.1$ are not located within the domain. The contour patterns are slightly different for the approximate values $\widetilde{\gamma}$, Figures 2c and 2f, as compared to their quadratic counterparts $\bar{\gamma}$, Figures 2b and 2e, but the same feature is observed, i.e. good agreement except for large growth rates above the dashed pink line of $\gamma/\nu_i = 0.5$.

From this analysis, a conservative estimate is that one can use approximate expressions as long as growth is slow $|\gamma| \leq 0.1$. This includes all marginal growth cases $\gamma = 0$. Moreover, numerical analysis presented in Figure 2 shows that one can relax this condition to $\gamma \leq 0.5$. This includes all E region cases of interest, Figures 2d–2f, and F-region cases with $G < 2 \times 10^{-4}$ m^{-1}, Figures 2b and 2c. The reason why the approximate expression (29) works at large negative values of γ is as follows. This expression is an approximation to the solution of quadratic equation (23) in which higher-order terms $\gamma^3\Gamma_3$ and $\gamma^4\Gamma_4$ have been neglected. They can become important, i.e. comparable with the dominant, linear term $\gamma\Gamma_1$, but only at very short scales. A simple OOM estimate shows that in the F-region, they are comparable near $\lambda = 0.05$ m, which is outside the wavelength range of interest (details are not presented here for brevity).

7. Explicit Expressions for the Oscillation Frequency

In this section, a set of approximate explicit expressions for the oscillation frequency and phase velocity is derived. We start from the quadric equation (11) and neglect higher-order terms $\gamma^3\Omega_3$ and $\gamma^4\Omega_4$, which results in the quadratic equation (in γ) of the form

$$\omega_r' D_0 = X\omega_{r0}' - \gamma\Omega_1 - \gamma^2\Omega_2, \tag{44}$$

where frequency-dependent quantities D_0, X, and Ω_j have been defined in Appendix A. This is next rewritten into an equivalent form

$$\omega_r' = \omega_{r0}' + \omega_r' \left(X - D_0\right) X^{-1} - \gamma\Omega_1 X^{-1} - \gamma^2\Omega_2 X^{-1}. \tag{45}$$

In terms with the growth rate γ in Eq. (45), we use the approximate expression (30) which is rewritten as

$$\gamma \approx \gamma_{\mathrm{FB}} + b\omega_r'\tau, \tag{46}$$

with newly defined quantities

$$\gamma_{\mathrm{FB}} \equiv \frac{\hat{\psi} r_i^{-1} \Omega_i^{-1} \left[\omega_r'^2 \left(1 - I^{-1}\right) - C_s^2 k_\perp^2\right]}{1 + \hat{\psi}\left(1 + I^{-1}\right)}, \qquad \tau \equiv r_i \frac{1 + I^{-1}}{1 + \hat{\psi}\left(1 + I^{-1}\right)}. \tag{47}$$

Here subscript FB is introduced to indicate that the first term in Eq. (46) refers to the pure Farley-Buneman instability case, while the second term is gradient-related through $b \propto G$. We also neglect all small terms $\propto G^2$ in the local approximation to obtain

$$\begin{aligned}
D_0 &\approx I + \hat{\psi}\left(1 + I\right) - b\omega_r' \Omega_i^{-1}\left(1 + I + 2\hat{\psi}\right), \\
X &\approx I + 2b\omega_r' \Omega_i^{-1}\left(\tau r_i - 1 + \tau \Omega_i^{-1} \gamma_{\mathrm{FB}}\right) + 2\gamma_{\mathrm{FB}} \Omega_i^{-1} r_i + \gamma_{\mathrm{FB}}^2 \Omega_i^{-2}, \\
X - D_0 &\approx b\omega_r' \Omega_i^{-1}\left(2\tau r_i - 1 + I + 2\hat{\psi} + 2\tau \Omega_i^{-1} \gamma_{\mathrm{FB}}\right) - \hat{\psi}\left(1 + I\right) + 2\gamma_{\mathrm{FB}} \Omega_i^{-1} r_i + \gamma_{\mathrm{FB}}^2 \Omega_i^{-2}, \\
\Omega_1 &\approx 2 r_i \omega_r' \Omega_i^{-1}\left(1 + 2\hat{\psi} + \hat{\psi}\kappa_{\mathrm{sc}}^2\right) + b\Omega_{1,b}, \\
\Omega_2 &\approx \omega_r' \Omega_i^{-2}\left(1 + 5\hat{\psi}\right) + b\Omega_{2,b},
\end{aligned} \tag{48}$$

where

$$\kappa_{\mathrm{sc}} \equiv \omega_r' \Omega_i^{-1} r_i^{-1}, \quad \Omega_{1,b} \equiv r_i\left[1 + I - 2\omega_r'^2 \Omega_i^{-2} + \hat{\psi}\left(1 + r_i^{-2} - 3\kappa_{\mathrm{sc}}^2\right)\right], \quad \Omega_{2,b} \equiv \Omega_i^{-1}\left(1 + 3r_i^2 + 2\hat{\psi}\right) \tag{49}$$

The next step is to approximate terms $\gamma\Omega_1$, $\gamma^2\Omega_2$ by using Eq. (46) for γ and expressions for Ω_j from Eq. (48) and, again, neglecting terms quadratic in $b \propto G$, with the resulting expression being

$$\begin{aligned}
\omega_r' &\approx \omega_{r0}' - b\omega_r'^2 \Omega_i^{-1}\left[1 - I - 2\hat{\psi} + 2\hat{\psi}\tau r_i\left(2 + \kappa_{\mathrm{sc}}^2\right) + 10\hat{\psi}\gamma_{\mathrm{FB}} \Omega_i^{-1}\tau\right] X^{-1}, \\
&- b\left(\gamma_{\mathrm{FB}}\Omega_{1,b} + \gamma_{\mathrm{FB}}^2 \Omega_{2,b}\right) X^{-1} - \hat{\psi}\omega_r'\left[1 + I + 2\gamma_{\mathrm{FB}} r_i \Omega_i^{-1}\left(2 + \kappa_{\mathrm{sc}}^2\right) + 5\gamma_{\mathrm{FB}}^2 \Omega_i^{-2}\right] X^{-1}.
\end{aligned} \tag{50}$$

The terms proportional to $\gamma_{\rm FB}$ and $\gamma_{\rm FB}^2$ can be neglected in Eq. (50) and X, since $\gamma_{\rm FB} \ll \nu_i$ (slow growth approximation) or, equivalently, $\gamma_{\rm FB}\Omega_i^{-1} \ll r_i$, $\gamma_{\rm FB}^2\Omega_i^{-2} \ll r_i^2 < I$, $\gamma_{\rm FB}\Omega_i^{-1} r_i \ll r_i^2 < I$. In addition, we neglect small terms $\propto \hat{\psi}$ in the second term in Eq. (50), with the resulting expression being

$$\omega_r' \approx \omega_{r0}' - \frac{b\omega_r'^2\Omega_i^{-1}(1-I) + \hat{\psi}\omega_r'(1+I)}{I + 2b\omega_r'\Omega_i^{-1}(\tau r_i - 1)}. \tag{51}$$

The OOM analysis shows that the second term in the denominator is considerable only in the F region at strong gradients $G > 10^{-3}$ m^{-1} and for most of cases of interest can be neglected. After rearranging Eq. (51), the final expression for the oscillation frequency is

$$\omega_r' \approx \widetilde{\omega}_r' = \frac{\omega_{r0}' + b\widetilde{\omega}_r'^2\Omega_i^{-1}\left(1 - \widetilde{I}^{-1}\right)}{1 + \hat{\psi}\left(1 + \widetilde{I}^{-1}\right)}, \quad \widetilde{I} \equiv r_i^2 + \widetilde{\omega}_r'^2\Omega_i^{-2}. \tag{52}$$

Here we introduced a new notation $\widetilde{\omega}_r'$ to differentiate from the exact value ω_r' and a corresponding quantity $\widetilde{I}$. One can see from Eq. (52) that, generally, $\omega_r' \neq \omega_{r0}'$. In the E region, $I^{-1} \ll 1$, and considering inequality (D6), Eq. (52) reduces to the expected value

$$\omega_r'^E \approx \frac{\omega_{r0}'}{1+\hat{\psi}}. \tag{53}$$

This is also consistent with $\omega_{r\vec{k}}'$ from Eq. (36). In a general case, Eq. (52) is a quadric equation on ω_r' since $I = r_i^2 + \omega_r'^2\Omega_i^{-2}$ which can be solved numerically. Alternatively, it can be solved iteratively and the first-order solution is

$$\omega_{r1}' = \frac{\omega_{r0}' + b\omega_{r0}'^2\Omega_i^{-1}\left(1 - I_0^{-1}\right)}{1 + \hat{\psi}\left(1 + I_0^{-1}\right)}, \quad I_0 \equiv r_i^2 + \omega_{r0}'^2\Omega_i^{-2}. \tag{54}$$

8. Limits of Applicability: Oscillation Frequency and Phase Velocity

The differences between frequencies calculated in the three approaches (zeroth-order ω'_{r0} using Eq. (13), approximate $\widetilde{\omega}'_r$ using Eq. (52), and first-order ω'_{r1} using Eq. (54)) are presented in Figure 3. It has the same format as Figure 2 except that the differences with respect to the exact values ω'_r normalized to ω'_{r0} are shown in all three columns, e.g. Figure 3a shows $(\omega'_{r0} - \omega'_r)/\omega'_{r0}$, Figure 3b shows $(\widetilde{\omega}'_r - \omega'_r)/\omega'_{r0}$, and Figure 3c shows $(\omega'_{r1} - \omega'_r)/\omega'_{r0}$. Since $\omega'_r/\omega'_{r0} = V_{\rm ph}/V_{\rm ph0}$, each panel also shows normalized differences between phase velocities. Since $V_{\rm ph0}$ is largely independent of G and λ, Figures 3a and 3d also show behavior of $V_{\rm ph}$ versus G and λ, e.g. green color refers to area where $V_{\rm ph} = V_{\rm ph0}$, while dark red contours of 0.1 refers to the line where $1 - V_{\rm ph}/V_{\rm ph0} = 0.1$ and hence where $V_{\rm ph} = 0.9V_{\rm ph0}$. In other words, green color shows areas where two approaches give the same result, while red color shows areas where zeroth-order values exceed exact ones significantly.

The first important feature in Figure 3a is that, in the F region, the zeroth-order result of ω'_{r0} considered in Section 3 generally applies only at weak gradients $G < 10^{-5}$ m^{-1} (green color). For stronger gradients, zeroth-order frequencies overestimate exact values $\omega'_{r0} > \omega'_r$. From Section 3, the zeroth-order phase velocity is approximately the plasma drift speed, $V_{\rm ph0} \sim V_d$, and the above result means that $V_{\rm ph} < V_d$. The ratio $V_{\rm ph0}/V_d$ is below 0.9 (red color) at $G = 10^{-4}$ m^{-1}.

Ideally, however, one would want to develop a method whose results differ not too much from the exact ones in a larger subset of the domain of interest. By solving Eq. (52) which is a quadric equation in $\widetilde{\omega}'_r$, one can largely achieve this goal, Figure 3b. Thus at long wavelengths $\lambda > 100$ m, small differences are now seen up to $G = 10^{-4}$ m^{-1}, while at 10 m they extend almost to $G = 10^{-3}$ m^{-1}. Interestingly, even the first-order results that are obtained by a simple substitution using Eq. (54), rather than solving a fourth-order equation (52), achieve similar results, Figure 3c. Here the blue area shift downwards as compared with Figure 3b, but overall the domain of applicability is much larger than in Figure 3a. An important subset is the area near $\gamma = 0$ (dashed line) where differences are small except for very short scales. This is expected since expressions for both $\widetilde{\omega}'_r$ and ω'_{r1} were developed for the slow-growth case. In the E region, the patterns are different, Figures 3d–3f, with the only area of large differences being where the local approximation fails (red corners and lines). This is also expected since the wave growth is slow in the domain of interest in the E region, while local approximation was also used in Section 7.

Finally, from the point of view of potential experimental signatures and verifications, it is important to consider how the applicability range in G changes versus wavelength λ. From Figure 3b, it is more extended at shorter scales than at longer scales. For example, this range in the F region is $G < 10^{-3}$ m^{-1} at $\lambda = 10$ m versus $G < 10^{-4}$ m^{-1} at $\lambda = 100$–1000 m. A similar feature is seen in the growth rate, Figure 2. Waves near $\lambda = 10$ m refer to the decameter-scale irregularities observed by coherent HF radars such as Super Dual Auroral Radar Network (SuperDARN) [e.g. *Chisham et al.*, 2007], while waves near 1000 m are thought to be responsible for scintillation of the radio signal in the Global Navigation Satellite System (GNSS) [e.g. *Basu et al.*, 1998; *Keskinen*, 2006]. This means that, under the strong gradient conditions, one has to be more careful in interpreting GNSS observations than those with SuperDARN. Unlike observations with coherent radars and GNSS receivers, numerical simulations provide information across a wide range of scales [e.g. recent studies by *Hassan et al.*, 2015, 2016; *Young et al.*, 2017, 2019], which is useful in considering wavelength dependence.

9. Stability Analysis and Role of Inertia

In this last section, we discuss various destabilizing and stabilizing factors and the role that the ion inertia plays in instability development for various altitudes. The approximate expression for the growth rate was derived in Section 4 as

$$\gamma \approx \frac{\hat{\psi}\nu_i^{-1}k^2\left[s_i r_i^2 V_E^2 \cos^2(\alpha+\beta)\left(1-I^{-1}\right)-C_s^2\right]+GV_E f s_i r_i^2\left(1+I^{-1}\right)}{1+\hat{\psi}\left(1+I^{-1}\right)}. \tag{55}$$

Generally, a quantity in the expression for the growth rate is considered destabilizing when it is positive and stabilizing if it is negative. For example, the diffusion term $-C_s^2$ in Eq. (55) is always negative and therefore stabilizing. Some factors may be either destabilizing or stabilizing, depending, for example, on vector orientation. For example, the second, GDI-related term in the numerator contains information about orientation in the angular function f; it is destabilizing for $f > 0$.

Eq. (55) is more suitable for such an analysis for arbitrary altitude than similar expressions that are written in terms of ω_r' or V_d since both are altitude-dependent, while factor $V_E = E_0/B$ is not. One example is the long-wavelength limit of the growth rate given by Eq. (55). In this case, the quantity I^{-1} simplifies to r_i^{-2} and the GDI term in Eq. (55) simplifies to $GV_E f$ since $s_i r_i^2\left(1+r_i^{-2}\right) = 1$. For the important special case of $\theta = 0$ ($\mathbf{V}_d \parallel \mathbf{k}$), Section 2, $f = 1$ and the growth rate is independent of altitude in the long-wavelength limit.

Figure 4 illustrates the growth rate behavior with the wavelength λ for various altitudes. From Figure 4, the growth rate approaches the same value at large λ, when it is normalized to GV_E. At short scales, the behavior is determined by the first term in the numerator $\propto k^2$. Depending whether the quantity in brackets is positive (110 and 120 km) or negative (altitudes ≥ 130 km), it increases or decreases with λ.

An important new result of this study is that the ion inertia plays a key role in the growth rate behavior by modifying other factors as discussed below. The dashed lines show dimensionless quantities $1 \pm I^{-1}$ that appear in Eq. (55) that deviate significantly from unity at long wavelengths. This deviation is important since the limit of $I^{-1} \to 0$ refers to the standard FBI/GDI mode, Eq. (34). Thus, Eqs. (30) and (55) may be regarded as a generalization of the standard FBI/GDI case for arbitrary altitude.

Another new result is that the ion inertia always amplifies the gradient effects. This is easy to see since the quantity I^{-1} is always positive and since $1 + I^{-1} > 1$ is multiplied by the gradient term $GV_E f$ in Eq. (55). As discussed above, when $f > 0$, this amplifies the destabilizing effects of gradients and when $f < 0$ their stabilizing effects are amplified.

In contrast, the quantity $1 - I^{-1}$ is always smaller than unity. Moreover, it can be negative, as for short scales $\lambda < 20$ m at 130 km and for all scales of interest at higher altitudes in Figure 4. The quantity $1 - I^{-1}$ is multiplied by the term $s_i r_i^2 V_E^2 \cos^2\theta$ in Eq. (55) which is also due to the ion inertia and in the E region, where $s_i r_i^2 \approx 1$, is traditionally associated with FBI. Thus additional inertial effects considered in the present study reduce this FBI factor and can even change a destabilizing FBI factor to a stabilizing one. The quantity $1 - I^{-1}$ reduces to $1 - r_i^{-2}$ at long wavelengths, which is consistent with *Dimant and Oppenheim* [2011b], Section 5.2, who also attributed this additional factor to the ion inertia. The current study thus may be regarded as an extension of the theory by *Dimant and Oppenheim* [2011b] to shorter scales.

The origin of the additional ion inertia effect is the higher-order terms in the dispersion relation. The quantity $I = r_i^2 + \omega_r'^2 \Omega_i^{-2}$ can be traced back to quantity $D_i = -i\Omega_i^{-1}\omega' + r_i$ that appears in the cubic dispersion relation (6). The standard FBI/GDI case can be obtained from an approximate version of the dispersion relation which is quadratic in D_i [*Makarevich*, 2016b], while consideration of the full cubic version for arbitrary altitude leads to our general case. As defined in Section 2, the quantity D_i is a Fourier representation of the convective derivative plus collisional term, while the cubic term D_i^3 can be traced back to the momentum equation whose solution for velocity includes both linear and nonlinear terms in D_i [*Makarevich*, 2016a, and their equations (11) and (12)]. In this sense one can regard additional inertial effects considered in the current study as "nonlinear", although one should not confuse those with nonlinear effects that are due to nonlinear terms in perturbations.

Finally, it is important to differentiate between the ion inertia itself that is represented by the quantity $I = r_i^2 + \omega_r'^2 \Omega_i^{-2} = \left(\nu_i^2 + \omega_r'^2\right) \Omega_i^{-2}$ and the effect considered here that is represented by its inverse $I^{-1} = \Omega_i^2 \left(\nu_i^2 + \omega_r'^2\right)^{-1}$. The often-used assumption of negligible inertia (e.g. at long wavelengths in the F region) results in small I, but large I^{-1} and hence large modification of the growth rate as compared to the standard FBI/GDI expression. In this limit, the modification actually results in the well-known simple F-region GDI expression GV_E. The quantity I^{-1} that appears in the arbitrary-altitude expressions (29),(30), and (55) thus facilitates a transparent reconciliation between different limiting cases.

10. Summary and Conclusions

1. The growth rate and oscillation frequency of unstable plasma waves generated by ionospheric plasma instabilities such the Farley-Buneman instability (FBI) and the gradient-drift instability (GDI) can be found from explicit expressions that are valid throughout the lower ionosphere including the ionospheric E and F regions.

2. The domains of applicability for the explicit expressions in terms of the plasma density gradient $\mathbf{G} = \nabla n/n$ and wavelength λ are controlled by the limits imposed by the local and slow growth approximations. In the E region, the expressions work for all scales of interest (G, λ), except at strong gradients and long wavelengths. In the F region, the applicability range in G changes with the wavelength λ; it is more extended at shorter scales than at longer scales. The obtained expressions apply for $G < 10^{-3}$ m^{-1} at $\lambda = 10$ m versus $G < 10^{-4}$ m^{-1} at $\lambda = 100$–1000 m. The commonly used assumption about the equivalency of the wave phase velocity V_{ph} and the plasma drift velocity V_d fails in the F region at gradients as weak as $G = 10^{-5}$ m^{-1}. A more careful treatment results in the ratio $V_{\mathrm{ph}}/V_d \approx 0.9$ at $G = 10^{-4}$ m^{-1} which decreases even further for stronger gradients.

3. The general explicit expressions represent a generalization of the standard FBI/GDI expressions in the E region to all altitudes, with previously-unreported additional effects due to the ion inertia represented by the factor $(\nu_i^2 + \omega_r'^2)^{-1}$. The additional inertial effect modifies the growth rate factors traditionally associated with FBI and GDI, with the FBI factor being reduced and the GDI factor being amplified. Progressively stronger effects are seen at larger altitudes and/or wavelengths. The previously-considered limiting cases (e.g. standard FBI/GDI mode) fall out transparently from the general expressions by considering magnitude of the additional inertial factor.

Appendix A: From Iterative to Quadric Form of Dispersion Relation

In this section, the iterative form of the dispersion relation (9) is rewritten into an alternative form with the growth rate $\gamma = \Im\omega'$ given explicitly everywhere. The alternative form is shown to be a quadric equation in γ that can be approximated into a linear or quadratic form in γ. By taking real and imaginary parts of Eq. (9), the following equations on the oscillation frequency ω_r' and the growth rate γ are obtained

$$\omega_r' = \Re\omega' = \frac{\omega_{r0}' + \gamma\left[\hat{\psi} r_i^{-1}\Im Z - \left(b + a\psi' r_i^{-1}\right)\Re Z\right]}{1 + \hat{\psi} r_i^{-1}\Re Z + \left(b + a\psi' r_i^{-1}\right)\Im Z}, \tag{A1}$$

$$\gamma = \Im\omega' = \frac{\hat{\psi} r_i^{-1}\left(-\omega_r'\Im Z - Ck_\perp^2\right) + \left(b + a\psi' r_i^{-1}\right)\omega_r'\Re Z}{1 + \hat{\psi} r_i^{-1}\Re Z + \left(b + a\psi' r_i^{-1}\right)\Im Z}, \tag{A2}$$

where

$$\omega_{r0}' \equiv \mathbf{V}_d \cdot \mathbf{k} - \left(b + a\psi' r_i^{-1}\right) Ck_\perp^2. \tag{A3}$$

Eqs. (A1) and (A2) are further rewritten as

$$\omega_r' = \frac{X\omega_{r0}' + \gamma\left[\hat{\psi} r_i^{-1} X\Im Z - \left(b + a\psi' r_i^{-1}\right) X\Re Z\right]}{X + \hat{\psi} r_i^{-1} X\Re Z + \left(b + a\psi' r_i^{-1}\right) X\Im Z}, \tag{A4}$$

$$\gamma = \frac{\hat{\psi} r_i^{-1}\left(-\omega_r' X\Im Z - XCk_\perp^2\right) + \left(b + a\psi' r_i^{-1}\right)\omega_r' X\Re Z}{X + \hat{\psi} r_i^{-1} X\Re Z + \left(b + a\psi' r_i^{-1}\right) X\Im Z}, \tag{A5}$$

where a new real quantity has been introduced

$$X \equiv |D_i - iaD_i + ib|^2 = X_2\gamma^2 + X_1\gamma + X_0, \tag{A6}$$

with

$$X_2 \equiv \Omega_i^{-2}\left(1 + a^2\right), \quad X_1 \equiv 2\Omega_i^{-1}\left(r_i + a^2 r_i - ab\right), \quad X_0 \equiv I\left(1 + a^2\right) + b^2 - 2abr_i - 2b\omega_r'\Omega_i^{-1}, \tag{A7}$$

$$I \equiv r_i^2 + \omega_r'^2\Omega_i^{-2}. \tag{A8}$$

Quantities $X\Re Z$ and $X\Im Z$ are found from Eq. (10) using definition of D_i in terms of ω' from Eq. (2)

$$X\Re Z = R_3\gamma^3 + R_2\gamma^2 + R_1\gamma + R_0, \tag{A9}$$

$$X\Im Z = I_3\gamma^3 + I_2\gamma^2 + I_1\gamma + I_0, \tag{A10}$$

with

$$R_3 \equiv \Omega_i^{-3},\ R_2 \equiv \Omega_i^{-2}\left(3r_i + a\omega_r'\Omega_i^{-1}\right),\ R_1 \equiv \Omega_i^{-1}\left[1 + I + 2r_i^2 + 2\left(ar_i - b\right)\omega_r'\Omega_i^{-1}\right],$$
$$R_0 \equiv \left(1 + I\right)r_i - a\omega_r'\Omega_i^{-1}\left(1 - I\right) - 2br_i\omega_r'\Omega_i^{-1}, \tag{A11}$$

$$I_3 \equiv a\Omega_i^{-3},\ I_2 \equiv \Omega_i^{-2}\left(3ar_i - b - \omega_r'\Omega_i^{-1}\right),\ I_1 \equiv -2r_i\Omega_i^{-1}\left(b + \omega_r'\Omega_i^{-1}\right) + a\Omega_i^{-1}\left(1 + I + 2r_i^2\right),$$
$$I_0 \equiv \omega_r'\Omega_i^{-1}\left(1 - I\right) + ar_i\left(1 + I\right) - b\left(1 + r_i^2 - \omega_r'^2\Omega_i^{-2}\right). \tag{A12}$$

Since both $X\Re Z$ and $X\Im Z$ are cubic in γ, both equations (A4) and (A5) are quadric in γ. After tedious but straightforward algebra, these can be rewritten into a form that is explicitly quadric

$$\omega_r' D_0 = \left(X_0 + X_1\gamma + X_2\gamma^2\right)\omega_{r0}' - \gamma\Omega_1 - \gamma^2\Omega_2 - \gamma^3\Omega_3 - \gamma^4\Omega_4. \tag{A13}$$

$$\gamma^4\Gamma_4 + \gamma^3\Gamma_3 + \gamma^2\Gamma_2 + \gamma\Gamma_1 = \Gamma_0, \tag{A14}$$

where quantities D_0, Ω_j, Γ_j are defined below and most are explicitly separated into parts proportional to different gradient powers, e.g.

$$D_0 \equiv D_{0,0} + D_{0,1} + D_{0,2}, \tag{A15}$$

with $D_{0,0} \propto G^0$ being a gradient-free term, $D_{0,1} \propto G$ (terms $\propto b \propto G$ and $a \propto G$), $D_{0,2} \propto G^2$ (terms $\propto b^2, a^2, ab$). The complete set of definitions is

$$D_{0,0} \equiv I + \hat{\psi}\left(1+I\right), \qquad D_{0,1} \equiv -b\left(1+I+2\hat{\psi}\right) + a\left(\psi' - \hat{\psi}\right) r_i^{-1}\omega_r'\Omega_i^{-1}\left(1-I\right),$$

$$D_{0,2} \equiv a^2\left[I + \psi'\left(1+I\right)\right] + abr_i\left(-1+I\right) - ab\psi' r_i^{-1}\left(1 + r_i^2 - \omega_r'^2\Omega_i^{-2}\right) + b^2\left(\omega_r'^2\Omega_i^{-2} - r_i^2\right), \tag{A16}$$

$$\Omega_{1,0} \equiv 2r_i\omega_r'\Omega_i^{-1}\left(1 + 2\hat{\psi} + \hat{\psi} r_i^{-2}\omega_r'^2\Omega_i^{-2}\right),$$

$$\Omega_{1,1} \equiv br_i\left(1 + r_i^2 - \omega_r'^2\Omega_i^{-2}\right) + b\hat{\psi} r_i^{-1}\left(1 + r_i^2 - 3\omega_r'^2\Omega_i^{-2}\right) + a\left(\psi' - \hat{\psi}\right)\left(1 + r_i^2 - \omega_r'^2\Omega_i^{-2}\right),$$

$$\Omega_{1,2} \equiv 2\omega_r'\Omega_i^{-1}\left[a^2 r_i + a^2\psi' r_i^{-1}\left(I + r_i^2\right) - 2b^2 r_i + ab\left(-1 + I + r_i^2 - 2\psi'\right)\right],$$

$$\Omega_{2,0} \equiv \omega_r'\Omega_i^{-2}\left(1 + 5\hat{\psi}\right), \qquad \Omega_{2,1} \equiv b\Omega_i^{-1}\left(1 + 3r_i^2 + 2\hat{\psi}\right) + a\Omega_i^{-1}\left(\psi' - \hat{\psi}\right) r_i^{-1}\left(1 + 3r_i^2\right),$$

$$\Omega_{2,2} \equiv \omega_r'\Omega_i^{-2}\left(a^2 + 5a^2\psi' - 3b^2 + 5abr_i - 3ab\psi' r_i^{-1}\right),$$

$$\Omega_3 \equiv 2\omega_r'\Omega_i^{-3}\left(\hat{\psi} r_i^{-1} + ab + a^2\psi' r_i^{-1}\right) + b\Omega_i^{-1}\left(\hat{\psi} r_i^{-1} + 3r_i\right) + 3a\Omega_i^{-1}\left(\psi' - \hat{\psi}\right),$$

$$\Omega_4 \equiv \Omega_i^{-3}\left[b + a\left(\psi' - \hat{\psi}\right) r_i^{-1}\right], \tag{A17}$$

$$
\begin{aligned}
\Gamma_{0,0} &\equiv \hat{\psi} r_i^{-1} \left[\omega_r'^2 \Omega_i^{-1} (I-1) - C k_\perp^2 I\right], \\
\Gamma_{0,1} &\equiv b\omega_r' r_i \left[1 + 2\hat{\psi} + I + \hat{\psi} r_i^{-2} \left(1 - I + 2Ck_\perp^2 \Omega_i^{-1}\right)\right] + a\omega_r' \left(\psi' - \hat{\psi}\right)(1+I), \\
\Gamma_{0,2} &\equiv \omega_r'^2 \Omega_i^{-1} \left[2b^2 r_i + a^2 \psi' r_i^{-1} (1-I) + ab(1 - I + 2\psi')\right] - \hat{\psi} r_i^{-1} C k_\perp^2 \left(a^2 I + b^2 - 2abr_i\right), \\
\Gamma_{1,0} &\equiv I + \hat{\psi}\left(1 + I - 2\omega_r'^2 \Omega_i^{-2} + 2Ck_\perp^2 \Omega_i^{-1}\right), \\
\Gamma_{1,1} &\equiv -2b\omega_r' \Omega_i^{-1} \left(1 + 2\hat{\psi} + r_i^2 + I\right) + 2a\left(\hat{\psi} - \psi'\right) r_i^{-1} \omega_r' \Omega_i^{-1} \left(I + r_i^2\right), \\
\Gamma_{1,2} &\equiv a^2 \left[I + \psi'\left(1 + I - 2\omega_r'^2 \Omega_i^{-2}\right) + 2\hat{\psi} C k_\perp^2 \Omega_i^{-1}\right] + b^2 \left(3\omega_r'^2 \Omega_i^{-2} - r_i^2\right), \\
&\quad + abr_i \left(-1 + I - 2\omega_r'^2 \Omega_i^{-2}\right) - ab\psi' r_i^{-1} \left(1 + r_i^2 - 3\omega_r'^2 \Omega_i^{-2}\right) - 2ab\hat{\psi} r_i^{-1} C k_\perp^2 \Omega_i^{-1}, \\
\Gamma_{2,0} &\equiv r_i \Omega_i^{-1} \left[2 + 3\hat{\psi} + \hat{\psi} r_i^{-2} \left(1 + Ck_\perp^2 \Omega_i^{-1}\right)\right], \qquad \Gamma_{2,1} \equiv \omega_r' \Omega_i^{-2} \left[5a\left(\hat{\psi} - \psi'\right) - br_i \left(5 + 3\hat{\psi} r_i^{-2}\right)\right], \\
\Gamma_{2,2} &\equiv 2r_i \Omega_i^{-1} \left(a^2 - b^2\right) + ab\Omega_i^{-1} \left(1 + 3r_i^2 - 2\psi' - 2\right) + a^2 \psi' r_i^{-1} \Omega_i^{-1} \left(1 + 3r_i^2\right) + a^2 \hat{\psi} r_i^{-1} C k_\perp^2 \Omega_i^{-2}, \\
\Gamma_3 &\equiv \Omega_i^{-2} \left(1 + 3\hat{\psi}\right) + 2\omega_r' \Omega_i^{-3} \left[a r_i^{-1} \left(\hat{\psi} - \psi'\right) - b\right] + \Omega_i^{-2} \left[a^2 (1 + 3\psi') - b^2 + ab\left(3r_i - \psi' r_i^{-1}\right)\right], \\
\Gamma_4 &\equiv \Omega_i^{-3} \left[\hat{\psi} r_i^{-1} + a^2 \psi' r_i^{-1} + ab\right].
\end{aligned}
\qquad \text{(A18)}
$$

The correctness of the quadric form expressions (A13) and (A14) has been verified by substituting numerical solutions of the cubic form (6) and determining that equations (A13) and (A14) hold to double precision (not presented here). It is for this reason that all terms including small ones were kept in Eqs. (A16)–(A18).

Appendix B: Differential Drift Velocity and Zeroth-Order Frequency

In this section, we evaluate $\mathbf{V}_d$ and ω_{r0}' for arbitrary altitude and vector directions. The previously derived general expressions for the drift velocities are [*Makarevich*, 2016a, equation (5)]

$$\mathbf{V}_{\alpha 0} = s_\alpha \left(\frac{\mathbf{E}_0}{B} - C_\alpha \mathbf{G} \right) \times \hat{\mathbf{b}} + s_\alpha r_\alpha \left(\frac{\mathbf{E}_{0\perp}}{B} - C_\alpha \mathbf{G}_\perp \right) + r_\alpha^{-1} \left(\frac{E_{0\parallel}}{B} - C_\alpha G_\parallel \right) \hat{\mathbf{b}}, \qquad \text{(B1)}$$

where $\mathbf{E}_0$ is the background electric field, $\mathbf{G} = \nabla n/n$ is the gradient strength vector, and

$$r_\alpha = \nu_\alpha/\Omega_\alpha, \qquad s_\alpha = \left(1 + r_\alpha^2\right)^{-1}, \qquad C_\alpha = T_\alpha/\left(q_\alpha B\right). \qquad \text{(B2)}$$

The differential drift velocity is found by subtracting the ion drift velocity from the electron drift velocity and rewriting

$$\begin{aligned} \mathbf{V}_d = s_e s_i \left(r_i - r_e\right)\left(1+\psi\right) \left(R\mathbf{V}_E - \frac{\mathbf{E}_{0\perp}}{B} \right) - \psi^{-1}\left(r_i - r_e\right) \frac{E_{0\parallel}}{B} \hat{\mathbf{b}} + \\ + s_e s_i \left(1+\psi\right) \Big[\left(C - RL\right) \mathbf{G} \times \hat{\mathbf{b}} + \left(RC + L\right) \mathbf{G}_\perp \Big] + \psi^{-1} L G_\parallel \hat{\mathbf{b}}. \end{aligned} \qquad \text{(B3)}$$

where

$$R \equiv \frac{r_i + r_e}{1+\psi}, \quad L \equiv r_i C_e - r_e C_i, \quad C = C_i - C_e. \qquad \text{(B4)}$$

This can be approximated for the case of fully-magnetized electrons $|r_e| \ll 1$ and $s_e \approx 1$ and for the ionospheric applications where $|r_e| \ll r_i$, $\psi \ll 1$. In this case, $R \approx r_i$, $C - RL \approx C - C_e r_i^2$, $RC + L \approx r_i C_i$, $\psi^{-1} L \approx -r_e^{-1} C_e$, and

$$\mathbf{V}_d \approx s_i r_i \left(r_i \mathbf{V}_E - \frac{\mathbf{E}_{0\perp}}{B} \right) + r_e^{-1} \frac{E_{0\parallel}}{B} \hat{\mathbf{b}} + s_i \Big[\left(C - C_e r_i^2\right) \mathbf{G} \times \hat{\mathbf{b}} + r_i C_i \mathbf{G}_\perp \Big] - r_e^{-1} C_e G_\parallel \hat{\mathbf{b}}, \qquad \text{(B5)}$$

A simple OOM analysis of V_d can be carried out by neglecting all terms except for the first one which includes two perpendicular components parallel to $\mathbf{V}_E$ and $\mathbf{E}_{0\perp}/B$. From these and definition of s_i from Eq. (B2),

$$V_d \sim s_i r_i V_E \left(r_i^2 + 1\right)^{1/2} = s_i^{1/2} r_i V_E. \qquad \text{(B6)}$$

The zeroth-order oscillation frequency defined by Eq. (13) is evaluated by approximating $a\psi' r_i^{-1} \ll b$, substituting Eq. (B5) and definitions of gradient terms a and b from Eq. (2), and simplifying

$$\omega'_{r0} \approx s_i r_i \left[r_i \left(\mathbf{V}_E - C_i \mathbf{G} \times \hat{\mathbf{b}} \right) - \left(\frac{\mathbf{E}_{0\perp}}{B} - C_i \mathbf{G}_\perp \right) \right] \cdot \mathbf{k} + r_e^{-1} k_\parallel \left(\frac{E_{0\parallel}}{B} - C_e G_\parallel \right). \quad \text{(B7)}$$

For realistic gradients $C_\alpha G \ll E_0/B$ and all gradient terms are negligible as compared to their electric field counterparts

$$\omega'_{r0} \approx s_i r_i \left(r_i \mathbf{V}_E - \frac{\mathbf{E}_{0\perp}}{B} \right) \cdot \mathbf{k} + r_e^{-1} k_\parallel \frac{E_{0\parallel}}{B}. \quad \text{(B8)}$$

One should note that the last step is only possible because both terms $\mathbf{V}_d \cdot \mathbf{k}$ and $bCk_\perp^2$ in ω'_{r0} contain gradient-dependent terms, but these partially cancel leaving only terms that can be neglected. A similar cancelation has been previously demonstrated by *Makarevich* [2016b] for the F-region case and purely perpendicular propagation $k_\parallel = 0$. For a more general case in the F region, $r_i \ll 1, s_i \approx 1$ and

$$\omega'^F_{r0} \approx -r_i \left(\frac{\mathbf{E}_{0\perp}}{B} \cdot \mathbf{k} + \psi^{-1} \frac{E_{0\parallel} k_\parallel}{B} \right). \quad \text{(B9)}$$

Appendix C: Growth Rate Expression: Order-of-Magnitude Analysis

In this section, we carry out an order-of-magnitude (OOM) analysis of two specific terms in the expression for the growth rate. It is demonstrated that the first term is important only at short wavelengths $\lambda < 10$ m in the F region, while the second term can be neglected for purely field-aligned irregularities (PFAI).

The explicit expression for the growth rate derived in Section 4 was as follows

$$\widetilde{\gamma} = \frac{\hat{\psi} r_i^{-1}\left[\omega_r'^2 \Omega_i^{-1}\left(1 - I^{-1}\right) - Ck_\perp^2\right] + b\omega_r' r_i \left(1 + I^{-1} + 2\hat{\psi} r_i^{-2} I^{-1} C k_\perp^2 \Omega_i^{-1}\right) + a\omega_r' \left(\psi' - \hat{\psi}\right)\left(1 + I^{-1}\right)}{1 + \hat{\psi}\left(1 + I^{-1}\right)}. \tag{C1}$$

The first term of interest is the term $2\hat{\psi} r_i^{-2} I^{-1} C k_\perp^2 \Omega_i^{-1}$ in the numerator. It is compared to the remaining terms $1+I^{-1}$ in the second term in the numerator in Eq. (29) by equating

$$2\hat{\psi} r_i^{-2} I^{-1} C k_\perp^2 \Omega_i^{-1} = \kappa\left(1 + I^{-1}\right), \tag{C2}$$

where κ is assumed to represent a smallness parameter, e.g. 0.01 or 0.1. From Eq. (C2), the wavelengths that refer to different κ levels are found by using an OOM estimate for ω_r' from Eq. (19) and a corresponding factor $I \sim r_i^2 + \Omega_i^{-2} s_i^2 r_i^2 V_E^2 k^2$. Under these approximations, Eq. (C2) becomes

$$2\hat{\psi} r_i^{-2} C k^2 \Omega_i^{-1} = \kappa\left(1 + r_i^2 + \Omega_i^{-2} s_i^2 r_i^2 V_E^2 k^2\right). \tag{C3}$$

When $\kappa\Omega_i^{-2} s_i^2 r_i^2 V_E^2 > 2\hat{\psi} r_i^{-2} C \Omega_i^{-1}$, there is no real solutions in k, which means that the left-hand-side is small for any k. This is the case for the E region. When $\kappa\Omega_i^{-2} s_i^2 r_i^2 V_E^2 < 2\hat{\psi} r_i^{-2} C \Omega_i^{-1}$, a solution is $k_\kappa^2 = \kappa s_i^{-1} / \left(2\hat{\psi} r_i^{-2} C \Omega_i^{-1} - \kappa\Omega_i^{-2} s_i^2 r_i^2 V_E^2\right)$, from which $\lambda_{\kappa=0.01} =$ 14 m and $\lambda_{\kappa=0.1} = 4.5$ m for the F region. This means that at scales near $\lambda \sim 10$ m and shorter, the term in question is important, but at longer wavelengths it quickly becomes negligible.

The second term is $a\omega_r' \left(\psi' - \hat{\psi}\right)\left(1 + I^{-1}\right)$, where $a = \mathbf{G} \cdot \mathbf{k}_\perp / k_\perp^2$ from Eq. (2). It is zero for purely perpendicular propagation $k_\parallel = 0$, since $\hat{\psi} = \psi' = \psi$ in this case from Eqs. (4) and (5). More generally, it can be neglected when $a\left(\psi' - \hat{\psi}\right) \ll br_i$. Since both gradient terms a and b are of the same magnitude and since $\psi' - \hat{\psi} \approx -r_i r_e^{-1} y^2$, this condition can be rewritten as $y^2 \ll -r_e$. This is significantly more restrictive than the condition of nearly field-aligned irregularities (NFAI) under which the general dispersion relation is valid. For arbitrary altitude, the NFAI condition is $y^2 \ll s_i r_i^2 < 1$, which in the F region can be written as $y^2 \ll r_i^2 \ll 1$, since $s_i \approx 1$ there. Thus the last term in Eq. (29) can be neglected close to purely perpendicular propagation or purely field-aligned irregularities (PFAI) when $y^2 \ll -r_e$.

In addition, this term is typically much smaller than the gradient-free term $\Gamma_{0,0} I^{-1} = \hat{\psi} r_i^{-1} \left[\omega_r'^2 \Omega_i^{-1} \left(1 - I^{-1}\right) - C k_\perp^2\right]$. A simple OOM analysis is to equate $a\omega_r' \left(\psi' - \hat{\psi}\right) = \hat{\psi} r_i^{-1} \omega_r'^2 \Omega_i^{-1}$ and to find the wavelength where the contributions are equal by utilizing OOM estimates $y^2 \sim -r_e$, $\psi' - \hat{\psi} \approx -r_i r_e^{-1} y^2 \sim r_i$, $\hat{\psi} = \psi \left(1 + r_e^{-2} y^2\right) \sim \psi \left(1 - r_e^{-1}\right) \sim r_i$, $a \sim b \sim G/k$, as well as Eq. (19) for ω_r'. With these estimates, the wavelength is found as $\lambda = 2\pi \sqrt{s_i V_E / G / \Omega_i}$, which for moderate gradients $G = 10^{-5}$ m^{-1} and strong convection $V_E = 1000$ m is $\lambda \sim 1000$ m for the E region and $\lambda \sim 3650$ m for the F region. This means that the term in question is small as compared to the gradient-free term $\Gamma_{0,0} I^{-1}$ except at long wavelengths in the E region.

Appendix D: Critical Gradients

The expressions for the growth rate can be analyzed analytically using various approaches, including analysis of the marginal instability growth condition $\gamma = 0$ and parameters such as electric field E and density gradients G that satisfy it [e.g. *Makarevich*, 2017]. In this section, a more general analysis is carried out in which gradient strengths G_κ are evaluated that are required to achieve a particular growth rate level κ, when normalized to the ion collision frequency ν_i

$$\gamma\left(G_\kappa\right)/\nu_i = \kappa, \tag{D1}$$

including critical gradients G_0 that lead to zero growth $\gamma\left(G_0\right) = 0$. It is useful to consider this more general case of G_κ rather than just G_0, since in developing expressions for the growth rate, the slow growth approximation was employed, Eq. (22). In this section, we will develop expressions for G_κ and then use these expressions in Section 6 to analyze limits of applicability of the developed expressions for the growth rate.

We start from Eq. (29), consider a case of the purely field-aligned irregularities (PFAI) where the last term in the numerator can be neglected, Appendix C, and substitute into Eq. (D1)

$$\kappa = \frac{\hat{\psi} r_i^{-2}\left[\omega_r'^2\Omega_i^{-2}\left(1-I^{-1}\right) - Ck_\perp^2\Omega_i^{-1}\right] + b\omega_r'\Omega_i^{-1}\left(1+I^{-1}+2\hat{\psi} r_i^{-2} I^{-1} Ck_\perp^2\Omega_i^{-1}\right)}{1+\hat{\psi}\left(1+I^{-1}\right)}. \tag{D2}$$

By substituting Eq. (31) into Eq. (D2) and rearranging, the exact expression for G_κ is

$$G_\kappa = \frac{\hat{\psi} r_i^{-2}\left[\omega_r'^2\Omega_i^{-2}\left(1-I^{-1}\right) - Ck_\perp^2\Omega_i^{-1}\right] - \kappa\left[1+\hat{\psi}\left(1+I^{-1}\right)\right]}{-\omega_r'\Omega_i^{-1}k_\perp^{-1}\sin\left(\alpha-\chi\right)\left(1+I^{-1}+2\hat{\psi} r_i^{-2} I^{-1} Ck_\perp^2\Omega_i^{-1}\right)}. \tag{D3}$$

The above expression can be approximated for the PFAI case by using Eq. (17) as

$$G_\kappa \approx -G_* f^{-1}\left(\alpha,\beta,\chi\right)\frac{\hat{\psi}\nu_i^{-2}k_\perp^2\left[s_i r_i^2 V_E^2\cos^2\left(\alpha+\beta\right)\left(1-I^{-1}\right) - C_s^2\right] - \kappa\left[1+\hat{\psi}\left(1+I^{-1}\right)\right]}{1+I^{-1}+2\hat{\psi} r_i^{-2} I^{-1} Ck_\perp^2\Omega_i^{-1}}, \tag{D4}$$

where function f has been previously defined by Eq. (33) and a new parameter G_* has been introduced as

$$G_* \equiv s_i^{-1} r_i^{-1} \Omega_i V_E^{-1}. \tag{D5}$$

The G_* parameter is a characteristic gradient strength which for our model parameters and strong convection case of $V_E = 1000$ m/s is 312 m at 300 km and 0.78 m at 110 km. For a weaker convection, it becomes smaller but still much larger than gradients within the range of interest $G = 10^{-8}$–10^{-2} m^{-1} so that $G \ll G_*$.

For future reference, it is also convenient to rewrite the combination $b\omega_r' \Omega_i^{-1}$ by using the same notations as

$$b\omega_r' \Omega_i^{-1} \approx G G_*^{-1} f(\alpha, \beta, \chi) \ll 1, \tag{D6}$$

where in the last inequality we used the previously obtained estimate $G \ll G_*$.

Acknowledgments. This work was supported by NSF grants AGS-1656955 and PLR-1443504. No data have been used in this theoretical study.

References

Basu, S., et al. (1998), Characteristics of plasma structuring in the cusp/cleft region at svalbard, *Radio Sci.*, *33*(6), 1885–1899, doi:10.1029/98RS01597.

Chisham, G., et al. (2007), A decade of the Super Dual Auroral Radar Network (SuperDARN): scientific achievements, new techniques and future directions, *Surveys in Geophysics*, *28*, 33–109, doi:10.1007/s10712-007-9017-8.

Dimant, Y. S., and G. M. Milikh (2003), Model of anomalous electron heating in the E region: 1. Basic theory, *J. Geophys. Res.*, *108*, 1350, doi:10.1029/2002JA009524.

Dimant, Y. S., and M. M. Oppenheim (2011a), Magnetosphere-ionosphere coupling through E region turbulence: 1. Energy budget, *J. Geophys. Res.*, *116*, A09303, doi: 10.1029/2011JA016648.

Dimant, Y. S., and M. M. Oppenheim (2011b), Magnetosphere-ionosphere coupling through E region turbulence: 2. Anomalous conductivities and frictional heating, *J. Geophys. Res.*, *116*, A09304, doi:10.1029/2011JA016649.

Fejer, B. G., D. T. Farley, B. B. Balsley, and R. F. Woodman (1975), Vertical structure of the VHF backscattering region in the equatorial electrojet and the gradient drift instability, *J. Geophys. Res.*, *80*, 1313–1324.

Fejer, B. G., J. Providakes, and D. T. Farley (1984), Theory of plasma waves in the auroral E region, *J. Geophys. Res.*, *89*, 7487–7494.

Hassan, E., W. Horton, A. I. Smolyakov, D. R. Hatch, and S. K. Litt (2015), Multiscale equatorial electrojet turbulence: Baseline 2-D model, *J. Geophys. Res. Space Physics*, *120*, 1460–1477, doi:10.1002/2014JA020387.

Hassan, E., D. R. Hatch, P. J. Morrison, and W. Horton (2016), Multiscale equatorial electrojet turbulence: Energy conservation, coupling, and cascades in a baseline 2-D fluid model, *J. Geophys. Res. Space Physics*, *121*, 9127–9145, doi:10.1002/2016JA022671.

Keskinen, M. J. (2006), GPS scintillation channel model for the disturbed low-latitude ionosphere, *Radio Sci.*, *41*(4), doi:10.1029/2005RS003442.

Makarevich, R. A. (2014), Symmetry considerations in the two-fluid theory of the gradient-drift instability in the lower ionosphere, *J. Geophys. Res.*, *119*, doi: 10.1002/2014JA020292.

Makarevich, R. A. (2016a), Toward an integrated view of ionospheric plasma instabilities: Altitudinal transitions and strong gradient case, *J. Geophys. Res. Space Physics*, *121*, 3634–3647, doi:10.1002/2016JA022515.

Makarevich, R. A. (2016b), Toward an integrated view of ionospheric plasma instabilities: 2. Three inertial modes of a cubic dispersion relation, *J. Geophys. Res. Space Physics*, *121*, 6855–6869, doi:10.1002/2016JA022864.

Makarevich, R. A. (2017), Critical density gradients for small-scale plasma irregularity generation in the E and F regions, *J. Geophys. Res. Space Physics*, *122*, 9588–9602, doi:10.1002/2017JA024393.

Press, W. H., S. A. Teukolsky, W. T. Vetterling, and B. P. Flannery (1992), *Numerical Recipes in Fortran 77: the Art of Scientific Computing. Second Edition*, vol. 1, Cambridge University Press.

Rogister, A., and N. D'Angelo (1970), Type II irregularities in the equatorial electrojet, *J. Geophys. Res.*, *75*, 3879–3887.

Sudan, R. N., J. Akinrimisi, and D. T. Farley (1973), Generation of small-scale irregularities in the equatorial electrojet, *J. Geophys. Res.*, *78*, 240–248.

Young, M. A., M. M. Oppenheim, and Y. S. Dimant (2017), Hybrid simulations of coupled Farley-Buneman/gradient drift instabilities in the equatorial E region ionosphere, *J. Geophys. Res. Space Physics*, *122*, 5768–5781, doi:10.1002/2017JA024161.

Young, M. A., M. M. Oppenheim, and Y. S. Dimant (2019), Simulations of secondary Farley-Buneman instability driven by a kilometer-scale primary wave: Anomalous transport and formation of flat-topped electric fields, *J. Geophys. Res. Space Physics*, *124*, 734–748, doi:10.1029/2018JA026072.

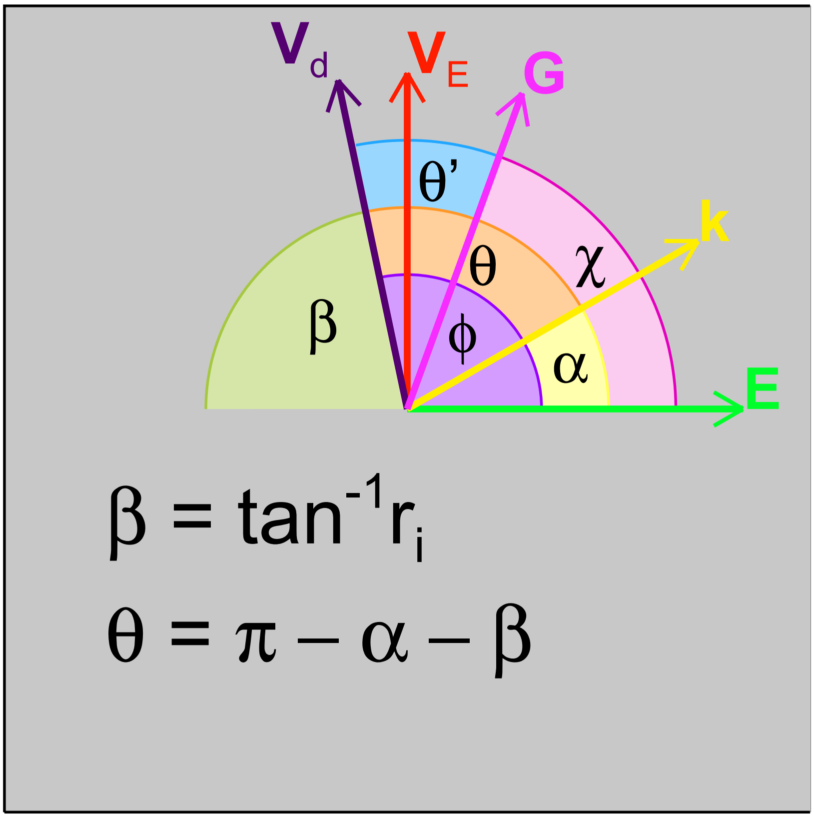

Figure 1. Vector geometry and angle definitions. Shown are the directions of the field-perpendicular components of the differential plasma drift velocity $\mathbf{V}_d$, the $\mathbf{E} \times \mathbf{B}$ drift velocity $\mathbf{V}_E$, gradient $\mathbf{G} = \nabla n/n$, wavevector $\mathbf{k}$, and the electric field $\mathbf{E}$. The definitions of six angles of interest are also shown. All angles are positive ccw from the x axis, except for β which is positive from the negative x axis cw.

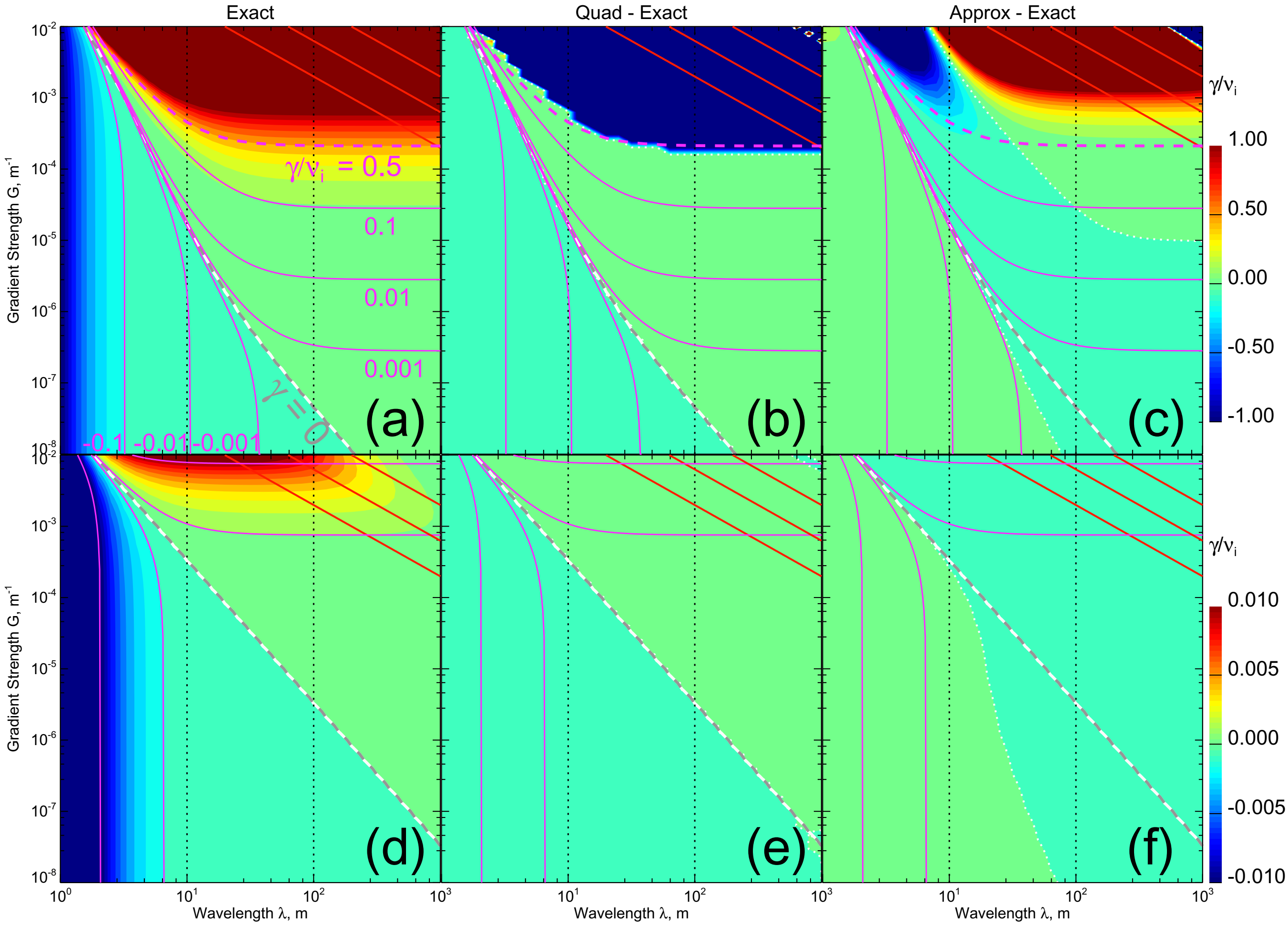

Figure 2. The growth rate dependence on the wavelength λ and gradient strength G for the gradient angle $\chi = \pi/2$, propagation angle $\alpha = 0$, and zero aspect angle $\alpha' = 0$. Shown are (a) the exact values γ normalized to ν_i, (b) differences between the quadratic values $\bar{\gamma}/\nu_i$ and the exact values γ/ν_i, and (c) differences between the approximate values $\widetilde{\gamma}/\nu_i$ and the exact values γ/ν_i at an F-region altitude of 300 km. Figures 2d–2f show the same but for an E-region altitude of 110 km. Also shown are the limits of applicability of the local ($G \ll k$; red lines) and slow-growth ($|\gamma| \ll \nu_i$; pink lines) approximations, as well as marginal instability conditions $\gamma = 0$ (grey-white dashed line), see text for details.

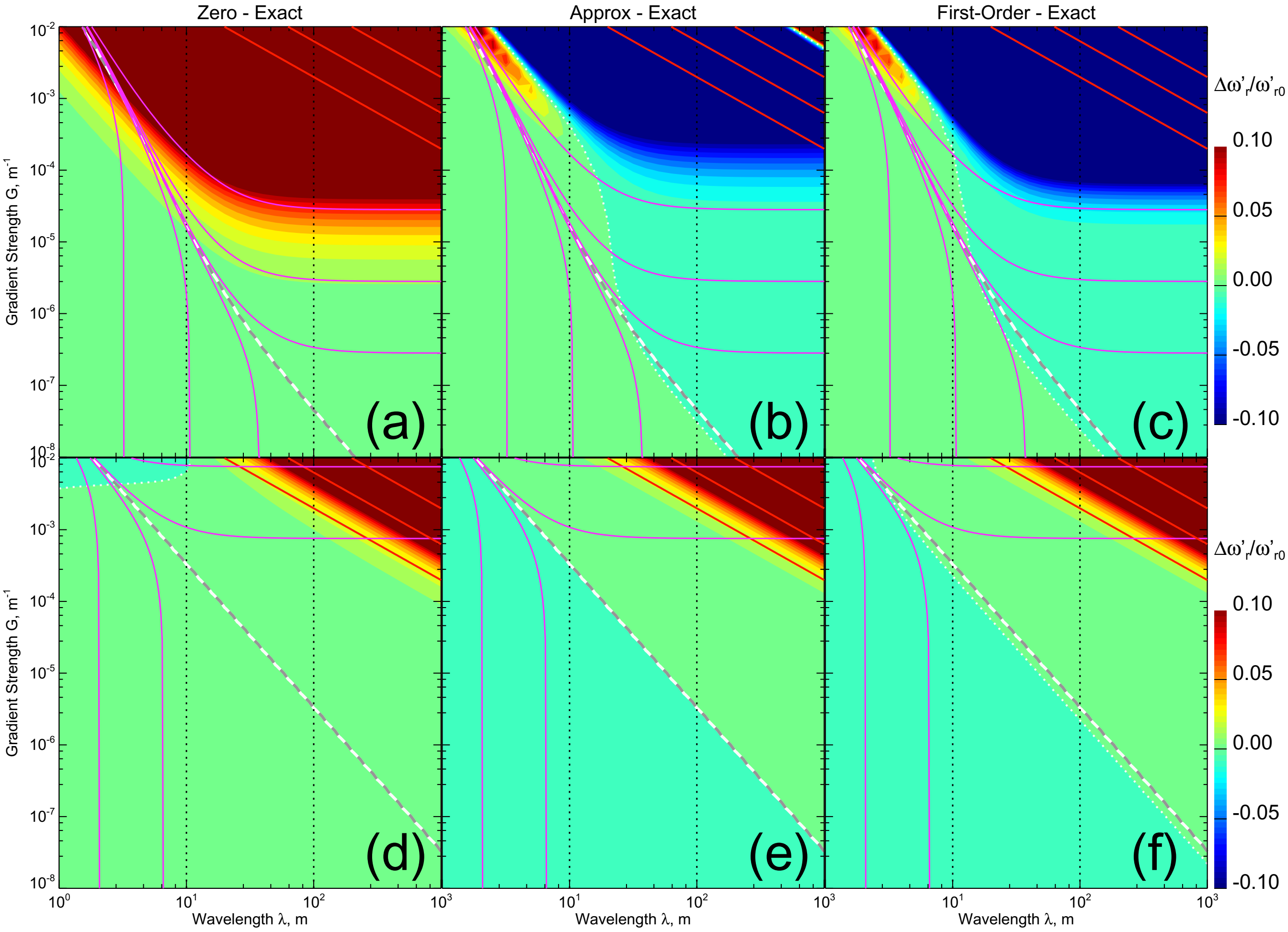

Figure 3. The same as Figure 2 but for the oscillation frequency. Shown are differences between (a) zeroth-order values ω'_{r0} and exact values ω'_r, (b) approximate quadratic values $\widetilde{\omega}'_r$ and exact values ω'_r, and (c) first-order values ω'_{r1} and exact values ω'_r at an altitude of 300 km normalized to ω'_{r0}. Figures 3d–3f show the same but at an altitude of 110 km. Since $\omega'_r/\omega'_{r0} = V_{\text{ph}}/V_{\text{ph0}}$, each panel also shows normalized differences between phase velocities.

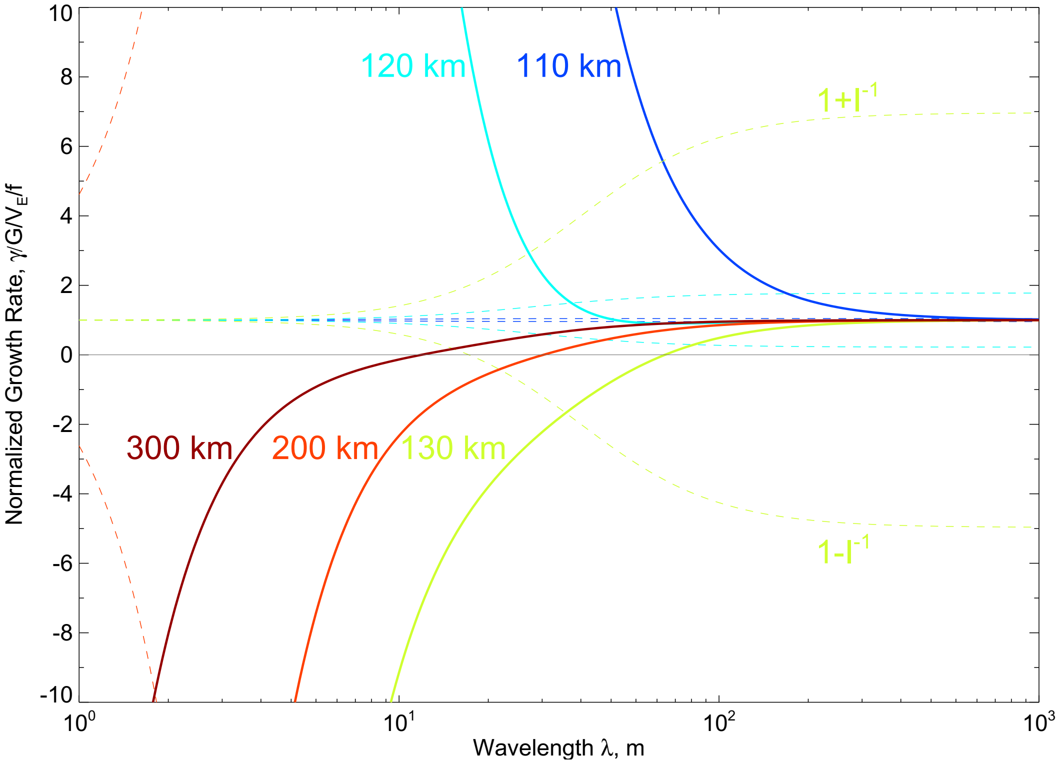

Figure 4. Normalized maximum growth rates $\gamma/(GV_E f)$ versus wavelength λ for $G = 10^5$ m^{-1} and $V_E = 1000$ m/s for 5 selected altitudes. Also shown by the dashed lines are dimensionless functions $1 \pm I^{-1}$.